small NANO MICRO

Force Spectroscopy

Molecular Recognition Force Spectroscopy: A New Tool to Tailor Targeted Nanoparticles

*Hugo Oliveira, Martina Rangl, Andreas Ebner, Barbara Mayer, Peter Hinterdorfer, and Ana P. Pêgo**

The density of targeting moieties in a nanoparticle-based gene-delivery system has been shown to play a fundamental role in its vectoring performance. Here, molecular recognition force spectroscopy is proposed as a novel screening tool to optimize the density of targeting moieties of functionalized nanoparticles towards attaining cell-specific interaction. By tailoring the nanoparticle formulation, the unbinding event probability between nanoparticles tethered to an atomic force microscopy tip and neuronal cells is directly correlated to the nanoparticle gene-vectoring capacity. Additionally, new insights into protein–receptor interaction are revealed. This novel approach opens new avenues in the field of nanomedicine.

1. Introduction

Gene therapy can be defined as a method that provides to somatic cells the genetic information required for producing specific therapeutic proteins in order to correct or modulate determined pathologies.[1] For most of the clinically relevant conditions, the expression of the delivered therapeutic gene should be constrained to a certain cell type. Extensive work has been developed in recent years to optimize and achieve successful gene delivery to mammalian cells. While targeted systems have primarily to interact with specific cell-surface molecules, most of the developed nonviral gene-delivery systems associate to cells by nonspecific interactions. In order to target nonviral gene-delivery vectors to specific cell populations, efforts have been made to combine targeting moieties to the surface of nanoparticles (see reference [2] for a review). We have recently developed vectors targeted to the peripheral nervous system (PNS) and showed that the density of ligand moieties plays an important role in the performance of the vectors.[3] However, the optimization of the density of targeting moieties implies tedious and time-consuming in vitro studies. Herein, we propose molecular recognition force spectroscopy (MRFS) as a novel screening tool to optimize the targeting moieties density of functionalized nanoparticles, towards attaining optimal cell-specific interaction. By tailoring the nanoparticle formulation, the unbinding event probability between nanoparticles and neuronal cells could be directly correlated to the nanoparticle gene-vectoring capacity. This novel approach can open important avenues not only in gene-delivery applications but also in the field of nanomedicine in general.

Dr. H. Oliveira, Dr. A. P. Pêgo
INEB–Instituto de Engenharia Biomédica
Divisão de Biomateriais
Universidade do Porto
Rua do Campo Alegre 823, 4150–180 Porto, Portugal
E-mail: apego@ineb.up.pt
M. Rangl, Dr. A. Ebner, B. Mayer, Prof. P. Hinterdorfer
Institute for Biophysics
Johannes Kepler Universität Linz
Altenbergerstrasse 69, 4040 Linz, Austria

DOI: 10.1002/smll.201002074

2. Results and Discussion

2.1. Grafting Chemistry

For MRFS experiments, single molecules are tethered to an atomic force microscopy (AFM) tip via flexible polyethylene glycol (PEG) linkers.[4,5] Here, we used as a model a previously defined polyethyleneimine (PEI) nanoparticle-based gene-delivery system bearing different amounts of a 50 kDa tetanus toxin fragment (HC) as targeting moiety.[3] Previously we have shown that the ligand moieties density plays a paramount role in the performance of these vectors targeted to the PNS.[3] In the present study, by using a hetero-bifunctional PEG_{18}, we were able to tether both the HC

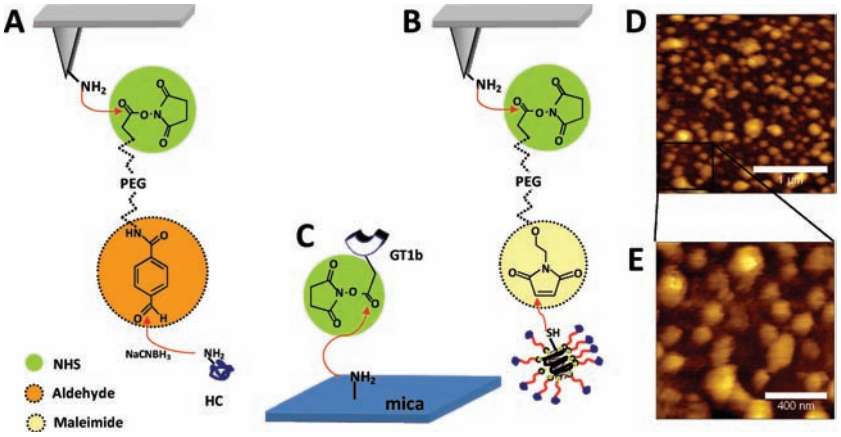

Figure 1. Schematic representation of the chemical tethering strategies used to bind the tetanus toxin fragment (HC fragment) (A) and the functionalized nanoparticles (B) to the AFM tip via a heterobifunctional PEG18. *N*-hydroxysuccinimide-activated GT1b trisialoganglioside receptor was grafted on mica (C). Both the tips and the mica were amino-functionalized using 3-aminopropyltriethoxysilane. The tethering of the nanoparticles was confirmed by imaging the surface of the cantilever using magnetic AC mode (D). Single nanoparticles could be resolved by AFM imaging (E).

fragment, via an aldehyde group, and the ternary nanoparticles, via a maleimide group (**Figure 1**A and B, respectively), to an AFM tip. The isolated trisialoganglioside GT1b receptor, which is reported to be specific for the HC fragment,[6] was grafted onto amino-functionalized mica (with 3-aminopropyltriethoxysilane according to Ebner et al.,[7] Figure 1C). Topographical AFM imaging of the cantilever chips was undertaken, using the magnetic AC (MAC) mode, to visualize the nanoparticle presence on the surface (Figure 1D). Single nanoparticles with an average diameter in the range of what has been previously determined by laser light scattering (63 ± 6 nm)[3] could be observed (Figure 1E, see Figure S1 in the Supporting Information (SI) for further details).

2.2. Force Measurements

Force–distance cycles were acquired by approaching the HC- or nanoparticle-modified tip to the GT1b-modified mica or cells, followed by its retraction. Nonspecific adhesion could be observed in the case of GT1b receptors on mica (**Figure 2**A,B). Nonetheless, the characteristic shape of the PEG-linker stretching allows the specific unbinding events to be distinguished from nonspecific adhesion.[4] Indeed, the interaction between ligand and receptor showed a characteristic nonlinear force signal for the four systems tested (Figure 2A–D).

The specific force signals were used to determine rupture forces and their accuracy for the previously described settings by calculating empirical probability density functions (PDFs), according to Baumgartner et al.[8] Representative PDFs for the different studied settings are presented in **Figure 3**. As observed in Figure 3A, the PDF of interaction between the HC fragment and the GT1b receptor presented a monomodal distribution with an unbinding event probability (UEP) of 16.2% at a retraction velocity of 600 nm s^{-1}. To prove that measured forces were due to specific interactions, surface blocking with free HC fragments was performed resulting in a drop of the UEP to 0.4%. In the case of nanoparticle–GT1b receptor interaction, a monomodal peak was also observed with a UEP of 22.0% at a retraction velocity of 500 nm s^{-1} (Figure 3B). Again, after blocking the UEP dropped to 2.4%, thus indicating the specificity of the measured forces.

For the specific interactions of the HC fragment and ND7/23 cells (neuronal cell line), the PDF showed a monomodal peak with a UEP of 16.2% (Figure 3C). The blocking with the HC fragment as well as in the control cells (NIH 3T3, fibroblasts) showed reduced UEP, 1.4 and 1.5%, respectively (Figure 3C). A monomodal peak was also observed in the case of the interaction of functionalized nanoparticles with ND7/23 cells with a UEP of 16.1% at a retraction velocity of 1000 nm s^{-1} (Figure 3D). Again the control

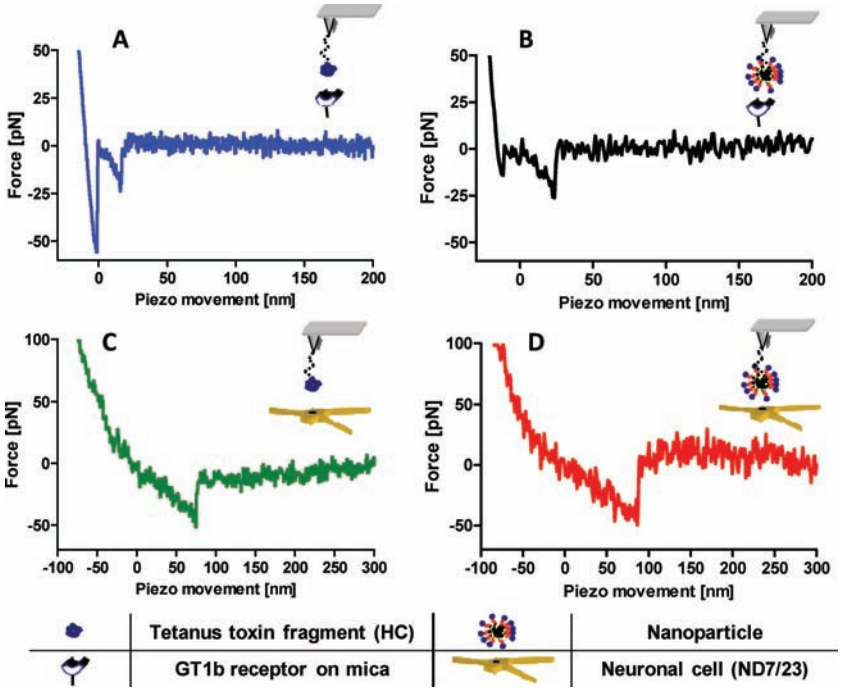

Figure 2. Force traces acquired with the AFM in force spectroscopy mode showing single molecular unbinding events. Typical force–distance retraces considering the interaction between the isolated tetanus toxin fragment (HC fragment) and GT1b trisialoganglioside receptor grafted on mica (A), functionalized nanoparticle and GT1b trisialoganglioside receptor (B), HC fragment and neuronal cell (C), and functionalized nanoparticle and neuronal cell (D).

small NANO MICRO

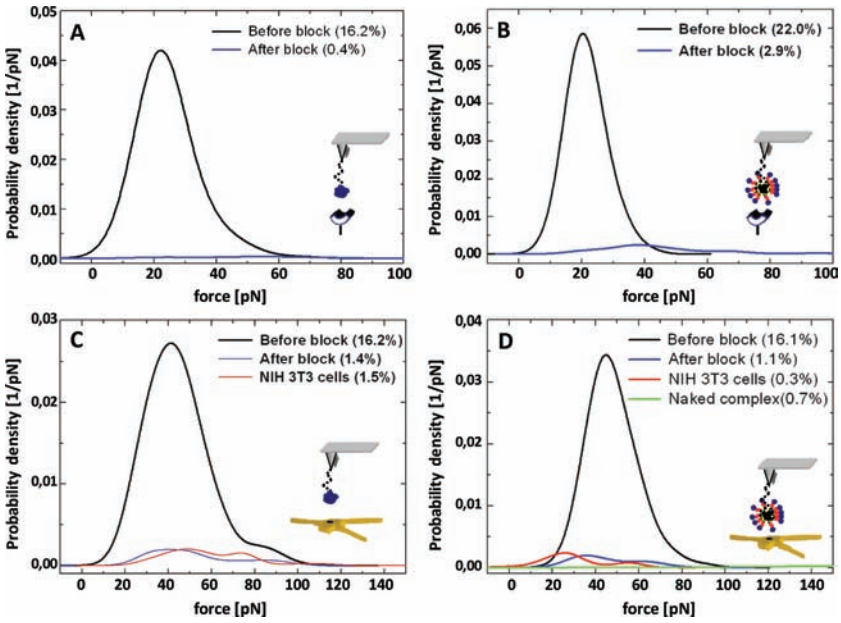

Figure 3. Probability density function (PDF) of rupture forces considering the interaction between the isolated tetanus toxin fragment (HC fragment) and GT1b trisialoganglioside receptor grafted on mica (A), functionalized nanoparticle and GT1b trisialoganglioside receptor (B), HC fragment and neuronal cells (C), and ternary nanoparticle and neuronal cell (D). In order to determine the specificity of the measured unbinding forces, controls were performed by surface blocking with free HC fragment (0.1 mg mL^{-1} for 1 h; after blocking), in the control cell line (NIH 3T3 cells) or using nanoparticles lacking the HC moieties (naked complex). The unbinding probability, before and after blocking (or other controls), are presented inside parentheses.

experiments point to the specificity of the measured forces, with a drop of the UEP being observed after blocking with free HC fragment, with the control cells, and when naked nanoparticles were used, with UEP values of 1.1, 0.3, and 0.7%, respectively (Figure 3D).

2.3. Loading Rate Dependence

Because molecular interaction forces depend on the timescale of the measurements,[9] unbinding forces were assessed at different retraction velocities (300 to 2000 nm s^{-1}). The unbinding forces were determined and the peak maxima plotted against the loading rate (r). The loading rate was calculated by multiplying the retraction velocity by the effective spring constant k_{eff}, which is the slope of the force–distance curve at rupture.[10] According to the theory that a single energy barrier is crossed in the thermally activated regime, a linear relation between the unbinding force and the logarithm of the loading rate is expected.[9,11] For the different conditions tested, a linear relation was observed (**Figure 4**). From this plot, and by fitting of Equation (1) (see Experimental Section and SI), the separation of the energy barrier in the direction of the force, x_β, and the kinetic off rate constant, k_{off}, can be determined.[9] For all tested conditions the x_β values were shown not to vary significantly (**Table 1**), as determined by a one-way ANOVA test considering a 95% confidence interval. In regard to the k_{off} values, and using the same statistical test, no statistically significant differences were found between the k_{off} values on cells (HC and nanoparticles; Table 1). By evaluating the interaction of isolated protein on isolated receptor versus the isolated HC on ND7/23 cells, we determined that both the unbinding forces and the average of ligand–receptor lifetime (given by k_{off}^{-1}) is higher in cells (Figure 4 and Table 1).

In this work we used as targeting moiety the HC fragment, which has been shown to interact specifically with peripheral neurons and to undergo retrograde transport.[12] It is well documented that GT1b gangliosides are required for interaction between HC and the neuronal cell surface to occur. However, this interaction was found to be protease sensitive, which suggests a dual receptor mechanism with an additional receptor being involved.[13] It is then expected that when the HC fragment interacts with the cell surface an association between the GT1b ganglioside receptor and the putative protein receptor occurs, thereby explaining the higher forces measured and increased interaction lifetime (k_{off}^{-1}). Additionally,

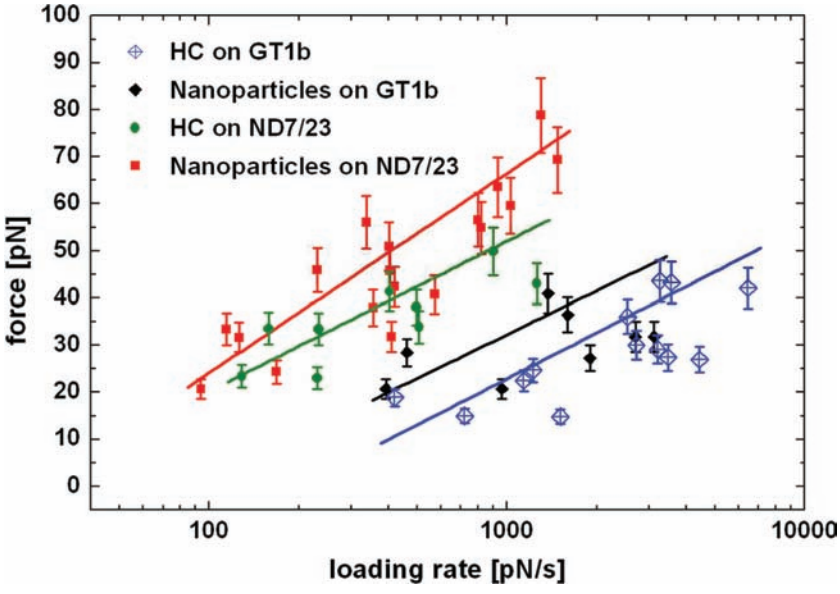

Figure 4. Loading rate dependence of the measured unbinding forces considering the interaction between: isolated tetanus toxin fragment (HC fragment) and GT1b trisialoganglioside receptor grafted on mica (blue diamonds), ternary nanoparticle and GT1b trisialoganglioside receptor (filled black diamonds), HC fragment and neuronal cells (ND7/23; green circles) and ternary nanoparticle and neuronal cell (red squares). The resulting fit (using Equation (1)) is shown by straight lines with the same correspondent color.

Table 1. From the fitting described in Figure 4, the position of the energy barrier along the direction of the force (x_β) and the kinetic off rate constant for the dissociation of the complex in solution (k_{off}) could be determined.

	x_β [Å]	k_{off} [s^{-1}]
HC on GT1b	2.91 ± 0.86	14.0 ± 5.53
Nanoparticles on GT1b	3.07 ± 1.42	6.71 ± 3.67
HC on ND7/23	2.97 ± 1.19	1.68 ± 1.05
Nanoparticles on ND7/23	2.24 ± 0.37	1.46 ± 0.42

significant differences were also found between k_{off} values of the HC or HC-functionalized nanoparticle interaction with the isolated GT1b receptor, despite the fact that the measured forces were of the same order of magnitude. This observation may be justified by the different steric environment that surrounds the HC protein when this is presented to the receptor tethered to the nanoparticles.

Although rare, multiple binding events could be observed in the case of the interaction between HC-functionalized nanoparticles and the isolated GT1b receptor (see Figure S2 in the SI). In the case of the interaction between nanoparticles and the ND7/23 cells multiple binding events were not observed, which indicated that the receptor density on cells was low and did not enable the occurrence of multiple HC fragment binding events.

2.4. Formulation Dependence on Nanoparticle–Cell Interaction

By using different nanoparticle formulations tethered on the tip and by performing force spectroscopy on the ND7/23 neuronal cell line, we aimed to study the influence of the density of targeting moieties on the binding probability. We observed that the nanoparticle targeting moieties density influences the nanoparticle binding probability to the ND7/23 cells (**Figure 5**A), although not having an impact on the measured forces (Figure 5B). The nanoparticle formulation prepared with 7.5 μg of HC-PEG per 2 μg of plasmid DNA elicits the higher binding probability outcome (Figure 5A), and it was also responsible for the higher transfection efficiency in cells (Figure 5C).

Our results show that for the desired targeting outcome, an optimal ligand density exists and, moreover, that surpassing this density results in a detrimental effect with the reduction of both the binding probability and the transfection efficiency (Figure 5A,B). The surface chain density and conformation of PEG are important factors that contribute to the "stealth" characteristics of PEGylated nanoparticles. At low targeting moieties density, most of the PEG chains have higher mobility and are closer to the surface of the particle ("mushroom" conformation).[14] However, as density increases the range of motion decreases, and most of the chains are extended away from the surface ("brush" conformation).[14] It is accepted that an optimal PEG coverage would be in between the mushroom and brushlike conformations, leading to an optimal surface steric hindrance.[15] In the present case, and although a decrease of binding probability was observed for the highest formulation, the measured forces did not suffer a significant variation throughout the formulations tested. We hypothesize that while the ligand density increases the associated PEG conformation also changes, and assumes a brushlike structure that can inhibit the spatial access of the cell receptors to the HC fragments, which explains the reduction of binding probability and transfection levels. Gu et al. have also reported that a narrowly defined targeting moieties density, with optimal outcomes in vitro and in vivo, could be obtained for aptamer-targeted nanoparticles for cancer applications.[16]

3. Conclusion

The optimal ligand density allowing maximal cell-specific interaction is a critical issue in the tailoring of targeted systems; however, new tools are awaited to assist in their efficient design. AFM has become a widely used tool for measuring both intra- and intermolecular interactions. Here we have proposed AFM as a screening tool for the efficient design of targeted nanoparticle systems. We were able to obtain new insights into the ligand–receptor mechanism and to determine the optimal targeted nanoparticle formulation regarding neuronal cell internalization and transfection. This new approach can find application in the growing field of nanomedicine.

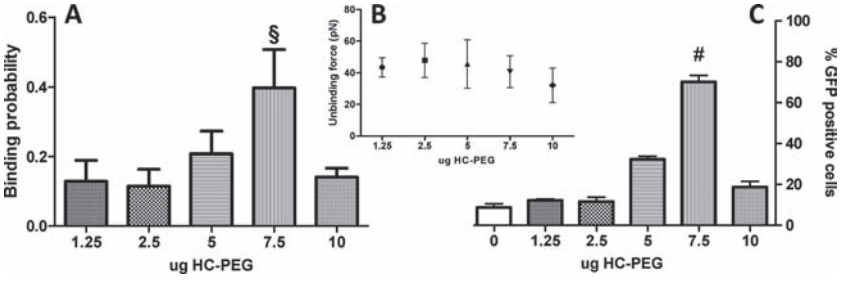

Figure 5. Influence of ligand density (expressed as micrograms of HC-PEG per 2 μg of plasmid DNA) on the binding probability on neuronal cells (ND7/23 cell line, A) and the correspondent force average values (B), percentage of green fluorescent protein (GFP) positive ND7/23 cells at 72 h post-transfection in relation to the nanoparticle formulation (average ± SD, C); A) each formulation considers the average of 9 data sets, with one data set corresponding to 1000 curves performed with a retraction velocity of 1000 nm s^{-1}; C) each formulation considers 20 000 events in flow cytometry ($n = 3$); § and # denotes statistical significant difference from other groups, $p < 0.05$, as determined by one-way ANOVA test followed by a Bonferroni's multiple comparison test).

4. Experimental Section

Polymer: Branched PEI (25 kDa, Sigma) was thiolated with 2-iminothiolane (Sigma) and purified as previously described.[3] The thiolated PEI (PEISH) was dissolved (1 mg mL^{-1}) in a 5% (w/v) glucose solution (pH 7.4) and stored at −80 °C until further use.

Plasmid DNA: The plasmid DNA used encoded for the green fluorescent protein (GFP; pCMV-GFP, 7.4 kb). Plasmid was produced in the DH5α competent *Escherichia coli* strain transformed with the respective plasmid. Subsequently, DNA purification was performed using an endotoxin-free Maxiprep kit following the manufacturer's instructions (GenElute, Sigma).

NANO MICRO small

Tetanus Toxin Production and Modification: The nontoxic fragment of the tetanus toxin (HC) was produced recombinantly using the BL21 *E. coli* strain. The plasmid encoding for the HC fragment was a kind offer from Prof. Neil Fairweather (King's College, UK). The HC production in the BL21 *E. coli* strain and its purification were performed as previously described.[12] The obtained HC fragment was covalently linked to a PEG spacer. Briefly, a heterobifunctional 5 kDa PEG (JenkemUSA, China) bearing an *N*-hydroxysuccinimide (NHS) and a maleimide (MAL) end group was used as indicated by the manufacturer, at a PEG/HC protein molar ratio of 2.5.[3]

Ternary Nanoparticle Formation: DNA–polymer complexes were prepared as described elsewhere by mixing, while vortexing equal volumes of plasmid DNA and PEISH solutions.[3] The core complexes were formed using PEISH at an N/P molar ratio of 3 and allowed to stabilize for 15 min. Subsequently, at a final concentration ranging from 1.25 to 10 μg per 2 μg of plasmid DNA, HC-PEG was added to the complex mixture and used immediately.

Gt1b Ganglioside Modification: The carboxylic moieties of the Gt1b ganglioside were activated using *O*-(*N*-succinimidyl)-1,1,3,3-tetramethyluronium tetrafluoroborate (TSTU) as follows. GT1b (0.5 mg; Sigma) was dissolved in dimethylformamide (DMF, 0.5 mL) and mixed with an equimolar solution (0.5 mL) of TSTU in DMF. Then, pyridine (0.5 mL) was added and the mixture was allowed to react for 3 h in an argon atmosphere, at room temperature (RT) with constant stirring. Pyridine was then evaporated (rotavap) and, subsequently, DMF was evaporated in liquid nitrogen for 1.5 h. The obtained product was dissolved in a 5:1 (v/v) chloroform/methanol solution and contaminants were extracted with Buffer A (100 mM NaCl, 50 mM NaH_2PO_4, 1 mM EDTA.Na_2, pH 7.5). The organic phase was dried and the obtained product was dissolved in DMF (0.5 mg mL^{-1}) and kept at –80 °C until further use.

Tip Chemistry: Commercially available silicon nitride AFM tips (Veeco Instruments) were amino functionalized using a gas-phase method with (3-aminopropyl)triethoxysilane (APTES, Sigma), as previously described.[7] The attachment of the HC fragment to the tip surface was achieved via a heterobifunctional PEG spacer, aldehyde-PEG-NHS (PEG_{18}), as previously described.[5] Briefly, the amino-functionalized tip was incubated in a correspondent linker solution (0.5 mL, 6.6 mg mL^{-1}) in chloroform (Sigma) with 2% (v/v) triethylamine (Sigma) for 2 h at RT. After rinsing twice in chloroform and drying in a N_2 flux, the tip was incubated for 1 h at 4 °C, in a solution of HC in phosphate-buffered saline (PBS; 0.1 mL at 0.2 mg mL^{-1}) with a $NaCNBH_3$ solution (2 μL, 1 M, prepared by adding 32 mg $NaCNBH_3$ to 500 μL 10 mM NaOH). Then, ethanolamine hydrochloride solution (5 μL, 1 M, pH 9.6) was added and incubation proceeded for 10 min at RT to block unreacted aldehyde groups. The tips were then washed three times with PBS and kept in PBS at 4 °C until further use. The attachment of the complexes to the tip surface was achieved via a heterobifunctional PEG spacer, MAL-PEG-NHS (PEG_{18}), as indicated below, and tested in close analogy to the aldehyde linker (data not shown). The amino-functionalized tip was incubated in the correspondent linker solution (0.5 mL at 2 mg mL^{-1}) in chloroform (Sigma) with 6% (v/v) triethylamine (Sigma) for 2 h at RT. After rinsing twice in chloroform and drying in a N_2 flux, the tip was incubated for 24 h at RT in a dispersion of complexes (0.1 mL) freshly prepared as described above. The tips were then washed in PBS three times and kept in PBS at 4 °C until further use.

Surface Chemistry: Freshly cleaved sheets of mica were amino functionalized by a protocol analogous to that described above.[7] The modified Gt1b solution was applied (30 μL) to each amino-functionalized mica sheet and then triethylamine (3 μL) was added before incubating 2 h at RT. After extensive washing with methanol, the sheets of mica were dried and kept in an N_2 atmosphere until further use.

Cell Lines: ND7/23 (mouse neuroblastoma (N18 tg 2) × rat dorsal root ganglion neurone hybrid) or NIH 3T3 (mouse embryonic fibroblast) cell lines (both obtained from ECACC) were routinely cultured in Dulbecco's Modified Eagle's Medium (DMEM) with Glutamax, supplemented with 10% (w/v) fetal bovine serum (FBS; heat inactivated at 57 °C for 30 min) and 1% PS (10 000 units mL^{-1} penicillin and 10 000 μg mL^{-1} streptomycin), all supplied by Gibco, and maintained at 37 °C in a 5% CO_2 humidified incubator. The ND7/23 cell line was chosen as a sensorial PNS cell model and the NIH 3T3 cell line as a fibroblast model. ND7/23 and NIH 3T3 cell lines were seeded at a cell density of 2.0×10^4 and 2.5×10^4 viable cells cm^{-2} (trypan blue assay), respectively, on glass coverslips coated with poly(D-lysine) (PDL, 0.1 mg mL^{-1}, Sigma) placed in a 24-well plate. Prior to AFM measurements, cells were fixed with 4% (w/v) paraformaldehyde in PBS for 15 min at RT and washed twice with PBS.

The evaluation of transfection efficiency, mediated by the functionalized nanoparticles in the proposed in vitro model, was of critical importance to better assess the impact of their targeting potential on their ability to promote higher levels of transfection in neuronal cells, as compared to naked nanoparticles. For transfection efficiency assessment, cells were transfected and analyzed 72 h post-transfection by flow cytometry for GFP expression with 20 000 gated events taken for each replicate ($n = 3$) as previously described.[3]

Force Measurements: All measurements were carried out in PBS using a PicoPlus (Agilent) AFM instrument. Force–distance cycles were performed at RT by using HC fragment- or complex-coated tips with 0.01–0.03 N m^{-1} nominal spring constants and mica-immobilized Gt1b receptor or glass-immobilized cells. Force–distance cycles were recorded at 0.5, 1, or 2 Hz vertical sweeping frequency and 300 nm *z*-range for measurements between HC fragment-coated tips and isolated receptors or 500 nm *z*-range for HC fragment- or complex-coated tips on isolated receptors or cells (see **Figure 6**).

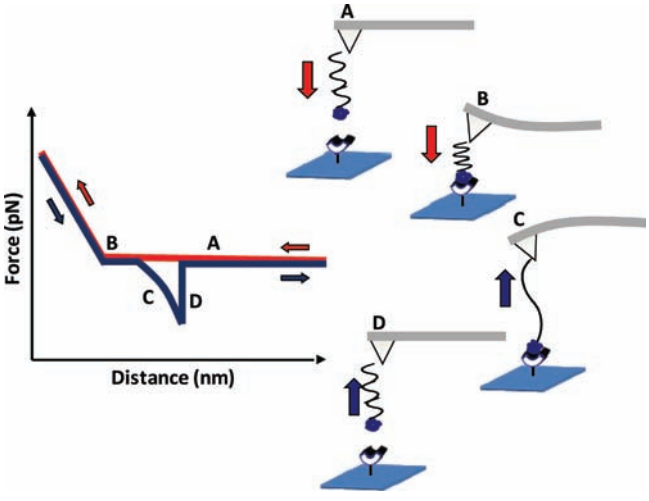

Figure 6. Schematic representation of a force distance cycle. The AFM tip approaches the sample surface (A). The ligand tethered to the tip encounters a receptor on the surface, and the tip applies a constant and default force upon the surface, thus resulting in cantilever deflection (B). Subsequently, the tip retracts from the surface leading to the stretching of the linker (nonlinear curve on the graph, C). Finally, enough force is applied to break the specific ligand–receptor bond, leading to a typical unbinding event (D).

For studies performed with complexes with different formulations, a 1 Hz vertical sweeping frequency at a 500 nm *z*-range were used. During one data set of 1000 force–distance curves, the tip position was changed by a few hundred nanometers several times to ensure that the binding events were statistically reasonable. The specificity of unbinding events was performed via the surface blockage with free HC fragment (0.1 mg mL^{-1} for 1 h). The spring constants of the cantilevers were determined by using the thermal noise method.[17,18] Empirical force distributions of the rupture forces of the last unbinding event (PDF) were calculated as previously described.[8] The loading rates were determined by multiplying the pulling velocity by the effective spring constant, that is, the mean slope at rupture. In the single-barrier model,[9] the most probable rupture force F^* is given as function of the loading rate r [see Equation (1)]:

$$F^* = \frac{k_B T}{x_\beta} \ln\left(\frac{r}{k_{off}\left(\frac{k_B T}{x_\beta}\right)}\right) \quad (1)$$

where k_B is the Boltzmann constant, T the absolute temperature, k_{off} the rate of dissociation of a ligand–receptor complex, and x_β the projection of the transition state along the direction of the force. The parameters x_β and k_{off} were determined by fitting F^* against ln r. The accuracy of the parameters was calculated by using propagation of errors assuming that the standard error of F^* is ≈15% (10% accounting for the spring constant determination and 5% to account for the uncertainty in determining the most probable rupture force), as previously described.[19]

Supporting Information

Supporting Information is available from the Wiley Online Library or from the author.

Acknowledgements

This project was carried out under the Portuguese Foundation for Science and Technology (FCT) contracts POCI/SAU-BMA/58170/2004 and PTDC/CTM-NAN/115124/2009 (the latter with co-funding from FEDER (FCOMP-01–0124-FEDER-014633)) as well as the Austrian Science Fond (FWF W1201 N13). H.O. acknowledges FCT for his PhD scholarship (SFRH/BD/22090/2005).

[1] I. M. Verma, M. D. Weitzman, *Annu. Rev. Biochem.* **2005**, *74*, 711–738.
[2] P. Midoux, G. Breuzard, J. P. Gomez, C. Pichon, *Curr. Gene Ther.* **2008**, *8*, 335–352.
[3] H. Oliveira, R. Fernandez, L. R. Pires, M. C. Martins, S. Simoes, M. A. Barbosa, A. P. Pego, *J. Controlled Release* **2010**, *143*, 350–358.
[4] P. Hinterdorfer, W. Baumgartner, H. J. Gruber, K. Schilcher, H. Schindler, *Proc. Natl. Acad. Sci. USA* **1996**, *93*, 3477–3481.
[5] A. Ebner, L. Wildling, A. S. Kamruzzahan, C. Rankl, J. Wruss, C. D. Hahn, M. Holzl, R. Zhu, F. Kienberger, D. Blaas, P. Hinterdorfer, H. J. Gruber, *Bioconjugate Chem.* **2007**, *18*, 1176–1184.
[6] C. Fotinou, P. Emsley, I. Black, H. Ando, H. Ishida, M. Kiso, K. A. Sinha, N. F. Fairweather, N. W. Isaacs, *J. Biol. Chem.* **2001**, *276*, 32274–32281.
[7] A. Ebner, P. Hinterdorfer, H. J. Gruber, *Ultramicroscopy* **2007**, *107*, 922–927.
[8] W. Baumgartner, P. Hinterdorfer, H. Schindler, *Ultramicroscopy* **2000**, *82*, 85–95.
[9] E. Evans, K. Ritchie, *Biophys. J.* **1997**, *72*, 1541–1555.
[10] E. Evans, K. Ritchie, *Biophys. J.* **1999**, *76*, 2439–2447.
[11] G. I. Bell, *Science* **1978**, *200*, 618–627.
[12] K. Sinha, M. Box, G. Lalli, G. Schiavo, H. Schneider, M. Groves, G. Siligardi, N. Fairweather, *Mol. Microbiol.* **2000**, *37*, 1041–1051.
[13] J. L. Halpern, A. Loftus, *J. Biol. Chem.* **1993**, *268*, 11188–11192.
[14] D. E. Owens III, N. A. Peppas, *Int. J. Pharm.* **2006**, *307*, 93–102.
[15] G. Storm, S. O. Belliot, T. Daemen, D. D. Lasic, *Adv. Drug Delivery Rev.* **1995**, *17*, 31–48.
[16] F. Gu, L. Zhang, B. A. Teply, N. Mann, A. Wang, A. F. Radovic-Moreno, R. Langer, O. C. Farokhzad, *Proc. Natl. Acad. Sci. USA* **2008**, *105*, 2586–2591.
[17] H. J. Butt, M. Jaschke, *Nanotechnology* **1995**, *6*, 1–7.
[18] J. L. Hutter, J. Bechhoefer, *Rev. Sci. Instrum.* **1993**, *64*, 1868–1873.
[19] C. Rankl, F. Kienberger, L. Wildling, J. Wruss, H. J. Gruber, D. Blaas, P. Hinterdorfer, *Proc. Natl. Acad. Sci. USA* **2008**, *105*, 17778–17783.

Received: November 17, 2010
Published online:

